NASA TECHNICAL MEMORANDUM

NASA TM X-52414

NASA TM X-52414

EFFECT OF COVER GAS PRESSURES ON ACCELERATED CAVITATION DAMAGE

by Stanley G. Young and James R. Johnston
Lewis Research Center
Cleveland, Ohio

TECHNICAL PAPER proposed for presentation at Pacific Symposia sponsored by the American Society for Testing and Materials
Honolulu, Hawaii, June 29-July 3, 1968

NATIONAL AERONAUTICS AND SPACE ADMINISTRATION · WASHINGTON, D.C. · 1968

EFFECT OF COVER GAS PRESSURES ON ACCELERATED CAVITATION DAMAGE

by Stanley G. Young and James R. Johnston

Lewis Research Center
Cleveland, Ohio

TECHNICAL PAPER proposed for presentation at

Pacific Symposia
sponsored by the American Society for Testing and Materials
Honolulu, Hawaii, June 29-July 3, 1968

NATIONAL AERONAUTICS AND SPACE ADMINISTRATION

EFFECT OF COVER GAS PRESSURES ON ACCELERATED CAVITATION DAMAGE

by Stanley G. Young and James R. Johnston

Lewis Research Center
National Aeronautics and Space Administration
Cleveland, Ohio

E-3860

SUMMARY

An investigation was made to study the effect of pressure on the resistance to cavitation damage of materials under consideration for components of liquid-metal power conversion systems. A vibratory apparatus was used to subject three materials, AISI 316 stainless steel, L-605, and Stellite 6B to accelerated cavitation damage in sodium at 800° F (700° K). Argon cover gas was used to maintain pressures up to 4 atmospheres (4×10^5 N/m^2) during test. Volume loss and volume-loss rate measurements were used to compare the effects of pressure on the degree of damage. Metallographic studies were conducted to determine the nature of damage.

Increasing cover-gas pressure significantly increased cavitation damage to all materials for all exposure times. The materials ranked in the same order with respect to resistance to cavitation damage at all pressures; Stellite 6B was most resistant, L-605 intermediate, and AISI 316 stainless steel least resistant. The steady-state volume-loss rate based on total specimen area increased linearly with cover-gas pressure. When the volume-loss rate data were normalized to include only the heavily damaged area of the specimens, the steady-state volume-loss rate increased as a power function of pressure. Metallographic examination of axially sectioned specimens revealed

undercutting and transgranular cracking as well as subsurface deformation for all materials.

INTRODUCTION

Components of advanced space power systems have shown cavitation damage in the form of pitting and surface erosion when tested for several hundred hours in liquid metal loops (refs. 1 to 3). Proposed power systems must function for 10 000 hours or longer and it is important to determine the resistance to cavitation damage of candidate materials in advance of service. Studies are being made of the resistance of materials to cavitation attack in liquid metals using accelerated types of laboratory tests, and considerable data describing material performance under cavitating conditions have been obtained. Some of the more recent of these investigations are described in references 4 to 6.

Extensive research is also being conducted to investigate the mechanism of cavitation and how the process causes material damage. Some of this work is presented in references 7 to 9. The process can briefly be described as follows: When local pressures in fluids fall below the fluid vapor pressure, cavities form. The pressure within a cavity or cavitation bubble is believed to be near the vapor pressure of the fluid (ref. 10). When these cavities are then subjected to regions of higher pressure, they collapse with high velocity. If the collapse occurs on a solid surface such as a metal, localized high pressures can be transmitted to the surface resulting in severe damage.

In power conversion systems, fluid pressures can vary, depending on the operating conditions, from near the fluid vapor pressures at the pump inlet to hundreds of psi at the pump outlet. Similarly in submersible vehicles for marine applications, ambient fluid pressures can increase significantly with depth. Therefore, it is important to establish the effect of pressure on cavitation damage to materials in order to achieve a better understanding of the cavitation phenomenon which is encountered in so many different engineering applications.

Some early studies were made to determine the effect of higher pressures on accelerated cavitation damage in water (ref. 11). These studies showed that increasing pressure up to 2 atmospheres (2×10^5 N/m^2) increased cavitation damage, but higher pressures up to 4 atmospheres (4×10^5 N/m^2) suppressed damage. Most other investigations of accelerated cavitation damage, have been performed at ambient pressures approximately equal to atmospheric pressure.

Greatly simplified, the difference between the local ambient pressure and the vapor pressure may be considered to be the net pressure or head available to collapse an existing cavitation bubble. The greater this pressure difference, or driving force, the higher will be the velocity of the fluid bubble wall impacting the surface. As a result, the impact force will be higher and the resulting cavitation damage will be greater. Isolating the pressure effect is thus extremely important in achieving a better understanding of the cavitation phenomenon. The problem is complicated by the interrelations among fluid temperature and pressure and material properties.

The purposes of this investigation were (1) to determine the effect of increasing ambient pressure on cavitation damage to materials in a vibratory test apparatus, (2) to compare the relative ranking of materials at both high and low pressures, and (3) to investigate some of the metallurgical aspects of cavitation damage.

In conducting this investigation, three materials with widely different mechanical properties were tested in sodium at 800° F (700° K) using a magnetostrictive vibratory apparatus. Argon cover gas was used over the liquid sodium to maintain pressures ranging from one to four atmospheres. Cavitation damage was determined by obtaining volume-loss measurements and by metallographic studies.

MATERIALS, APPARATUS, AND PROCEDURE

Materials

The materials investigated were AISI type 316 stainless steel, and the cobalt-base alloys, L-605 (HS-25) and Stellite 6B. These three materials were chosen because of the wide differences they exhibited to cavitation damage in sodium at atmospheric pressure (ref. 4). AISI type 316 stainless steel showed low resistance to cavitation damage. L-605 showed intermediate resistance to damage. Stellite 6B was the most damage resistant alloy. The nominal chemical composition of each alloy is listed in table I. The heat treatments, densities, and mechanical properties are given in table II.

Reactor grade sodium (99.95 percent purity) was used as the test fluid. Chemical analyses indicated an initial oxygen level of less than

10 ppm for the sodium. Purity of the sodium was maintained by the addition of a titanium-sponge hot trap to the liquid-metal bath.

Accelerated Cavitation Damage Test Facility

The apparatus used is shown schematically in figure 1. A complete description of the facility and test procedure is given in reference 4. Figure 1 illustrates the vacuum dry-box arrangement, magnetostrictive transducer assembly, and separately sealed liquid-metal test chamber with associated argon line, vapor trap, and pressure gage. The dry box and test chamber were evacuated to a pressure of approximately 10^{-3} torr (0.13 N/m^2) and backfilled with high purity argon prior to testing.

The specimen was attached to the end of a resonant system consisting of a transducer, exponential horn, and an extension-rod specimen holder. The amplitude and frequency of vibration were detected by a magnetic pickup, and read on an oscilloscope. An automatic feedback system maintained constant amplitude irrespective of variations in resonant frequency induced by temperature changes.

When the transducer assembly was lowered into position, a sleeve attached to the nodal flange on the amplifying horn sealed the liquid-metal test chamber from the dry box, and the test chamber pressure was regulated through a separate argon line. Pressures were measured with a precision pressure gage having an accuracy of 0.25 percent.

Test Conditions

The test conditions for each material are listed in table III. All tests were run in sodium at $800^{\circ} \pm 10^{\circ}$ F (700° K); the vapor pressure of sodium at this temperature is 0.015 psia (1.03×10^{2} N/m^{2}) (ref. 12). The frequency of vibration of the test specimens was nominally 25 000 Hz, and the peak to peak displacement amplitude was 0.00175 ± 0.00005 inch (4.45×10^{-2} mm). The specimen surface was immersed to a depth of approximately 0.13 inch (3.3 mm).

Test Procedure

The type of a specimen used is shown in figure 2. The test surface of each specimen was metallographically polished before test to allow meaningful examination of the specimen surface at high magnification during the early stages of damage. Prior to the test, the specimens were weighed and photographed. After each period of operation, the specimens were cleaned, weighed and rephotographed. Weight-loss measurements were divided by density to obtain volume loss.

Test duration was dependent on the volume-loss rate of each specimen. In most cases, the testing of a specimen was stopped after it maintained a relatively constant volume loss between weighings.

After testing, the specimens were sectioned axially and examined metallographically to determine the depth of cavitation attack and to study any reaction zones that might exist between the sodium and the specimen material.

CAVITATION DAMAGE RESULTS

Cavitation damage, expressed as cumulative volume loss and as volume-loss rate is plotted against time for each material tested in figures 3 to 5. The effect of pressure on the rate of cavitation damage is plotted in figures 6 and 7. Cavitation damage data are also summarized in table IV. The results of metallographic studies are presented in figures 8 to 13.

Volume Loss and Volume-Loss Rate

The cavitation damage to L-605 at 1, 2, 3, and 4 atmospheres (1, 2, 3, and 4×10^5 N/m^2) is shown as volume loss and as volume-loss rate in figures 3(a) and (b), respectively. Volume-loss rate curves were obtained by dividing the volume loss between successive weighings by the increment of test time between them. These values were then plotted midway between the weighing times. From figure 3, it is evident that cavitation at higher pressures results in (1) higher cumulative volume loss, (2) a higher volume-loss rate peak, and (3) a higher level of steady-state volume-loss rate. The steady-state region is defined in this investigation as the zone of minimum volume-loss rate after the damage rate has passed through a peak. In this region, the volume-loss rate does not change significantly over an extended period of time, and values for a relatively steady-state damage rate can be determined. It is interesting to note that the shape of the rate curve varies with pressure (fig. 3(a)). As the pressure is increased, the peak of the damage rate curve is higher and narrower and occurs earlier.

During the one atmosphere test, the first L-605 specimen tested failed at the threaded joint after 90 minutes exposure. The test was repeated with a second specimen and continued for 360 minutes. Damage was slight during the first 90 minutes, and the data were virtually identical for the two specimens. Consequently, one smooth curve was drawn through the data. At 3 atmospheres (3×10^5 N/m^2), a similar specimen failure occurred after 120 minutes. A second specimen was therefore run and the test continued for a total 360 minutes. Because the cumulative volume loss of the two specimens run at the same pressure showed a difference of about 10 cubic millimeters at the 120 minute point, separate curves are plotted in figure 3.

Figure 3(b) shows that the volume-loss rate curves increase for the specimens tested at 3 and 4 atmospheres (3×10^5 and 4×10^5 N/m^2) after 240 minutes. This increase is most likely due to undercutting of the surface by cavitation and the resultant loss of large particles of material. Some large particles of specimen material were found in the sodium bath. Further evidence of such undercutting is presented in the section dealing with the metallographic studies.

Volume loss and volume-loss rate curves are shown in figure 4 for AISI type 316 stainless steel at 1, 2.7, and 4 atmospheres (1, 2.7, and 4×10^5 N/m^2). Similar curves for Stellite 6B are shown in figure 5. Increasing the test pressure increased the cumulative volume loss in each case and both materials exhibited steady-state volume-loss rates that increased with increasing pressure. However, the volume-loss

rate peaks were not as well defined as for the L-605 specimens (fig. 3(b)).

The effect of pressure on the volume loss of the Stellite 6B specimens was not as clearly defined as in the case of the other materials. There is relatively little spread between the 2.7- and 4- atmosphere (2.7×10^5 and 4×10^5 N/m^2) test results. The unusual behavior of this material may be due, in part, to the changing patterns of the damage. This will be discussed further in the section on metallography. Although there is an overlap of the rate curves for Stellite 6B (fig. 5(b)), the peak damage rate and steady-state damage rate increase with increasing test pressure.

Relation Between Steady-State Volume-Loss Rate and Pressure

The steady-state volume-loss rates for L-605, AISI 316 stainless steel and Stellite 6B determined from figures 3(b), 4(b), and 5(b), respectively, are listed in table IV. These values are plotted against pressure in figure 6. When it is assumed that cavitation damage can be expressed by the steady-state volume-loss rate of a material, damage increases linearly with ambient pressure for the pressure range considered. Of course, under other test conditions (different amplitudes of vibration, temperature, specimen size, etc.) this relation might not hold true. It is important to note that the resulting linear relation is based on the conventional method of measuring cavitation damage which does not take into account the damage pattern.

From the photographs of figures 8 to 11, it is obvious that there is an area of heavy damage, and a surrounding area of little or no damage on the tested specimens. The heavily damaged area was reduced in size but the depth of damage increased as the cover-gas pressure was increased. If the volume-loss rate data are normalized on the basis of damaged area only, the effect of pressure on volume-loss rate will no longer be linear, but volume-loss rate will vary as a power of pressure. The normalized cavitation damage data are listed in table V and plotted in figure 7. In figure 7, the slopes of the curves for AISI 316 stainless steel, L-605, and Stellite 6B are 2.0, 2.2, and 2.7, respectively.

The results of the present investigation differ from those obtained by previous investigators (ref. 11). Using a low-frequency (6500 Hz) magnetostrictive device in water, they found that for a given exposure time, damage increased with increasing pressure up to about 2 atmospheres (2×10^5 N/m^2) and subsequently decreased as pressure was further increased. No damage was observed at 4 atmospheres (4×10^5 N/m^2). It may be that, because the apparatus used for the eariler tests (ref. 11) had a relatively low frequency resulting in relatively low fluid velocities, cavitation was greatly reduced at the higher ambient pressures. The high-frequency device used in the present investigation is, however, capable of generating cavitation at these higher ambient pressures.

From figures 6 and 7, it is apparent that materials have the same relative ranking with respect to cavitation damage resistance at high

pressures that they have at atmospheric pressure. Accelerated material damage tests, therefore, may be run at higher ambient pressures, and test time can be shortened by at least an order of magnitude.

An AISI 316 stainless-steel specimen was run for a test time of 16 hours at 0.5 atmosphere. During the last 8 hours of this test, the specimen had a steady-state damage rate of approximately 0.5 cubic millimeter per hour. This value is also plotted on figure 6. It is believed that a zero damage rate occurs when cover-gas pressure is very near the vapor pressure of the fluid.

It can be observed from figure 6 that the cruves for more severly damaged materials have the steeper slopes, and it would appear that the relative effect of pressure on the damage rate is greater for the less resistant materials. If, however, the data are normalized (fig. 7), this trend is reversed; that is, the curves of the more resistant materials have steeper slopes and the relative effect of pressure on the damage rate is greater for the more resistant materials.

Metallography

Macrographs were taken of all the specimens tested. The damaged surfaces of L-605 specimens are illustrated in figure 8. After only 15 minutes severe damage is evident in specimens exposed at 4 atmospheres (4×10^5 N/m^2); whereas, the specimens exposed at 1 atmosphere (1×10^5 N/m^2) show very little damage even after 60 minutes of testing.

Several large projections can be seen in the central portion of the surfaces of specimens exposed for 360 minutes at 3 and 4 atmospheres (3×10^5 and 4×10^5 N/m^2). Undercutting and loss of such projections are believed to be the reason the volume-loss rate curves (fig. 3(b)) showed an increase at the longer exposure times. Evidence of undercutting is apparent in the macrographs of figure 9. This figure clearly shows the increasing depth and amount of attack with increasing pressure. Wider undamaged rims and greater undercutting are evident in the specimens tested at higher pressures. Calculated areas of heavy damage are shown in table V.

Damaged surfaces of 316 stainless steel and Stellite 6B specimens are shown in figures 10 and 11, respectively. As in the case of L-605, damage at 4 atmospheres (4×10^5 N/m^2) was much more severe than that at 1 atmosphere (1×10^5 N/m^2), and damage was primarily concentrated in the central region of the specimens. The AISI 316 stainless-steel specimen sustained such a severe attack at 4 atmospheres (4×10^5 N/m^2) that even portions of the rim were damaged. Although not shown, the heavily damaged specimens of AISI 316 stainless steel and Stellite 6B were also sectioned and macrographs were taken. These had a similar appearance to the sectioned L-605 specimens shown in figure 9.

Photomicrographs were taken of the surfaces of the L-605 specimens in the early stages of cavitation attack. These together with the original microstructure of an L-605 specimen are shown in figure 12.

The specimen was electrolytically etched with a solution of hydrochloric acid (30 ml) and hydrogen peroxide (3 drops), and was repolished before testing. Specimens tested at pressures above 2 atmospheres (2×10^5 N/m^2) were damaged too severely to show significant features under high magnification. In all cases during the early stages of damage, attack along grain and twin boundaries was noted.

Figure 13 shows photomicrographs of sectioned specimens of all materials before and after testing. All the materials tested exhibited gross undercutting and transgranular cracking. Evidence of subsurface deformation existed in the form of slip bands for all materials. Bending of twin boundaries was observed in L-605 (fig. 13(a)). Breaking of subsurface carbides in Stellite 6B is apparent in figure 13(c). No evidence of any reaction zone was found in the cavitation damaged regions of any specimen.

Comparison of Accelerated Cavitation Damage and Pump Impeller Test Results

An interesting example of the effect of pressure on cavitation damage to a pump impeller operated in a liquid metal has been reported in reference 1. In this investigation, an impeller of AISI 316 stainless steel was operated first in water at room temperature then in potassium at 1400° F (1033° K). Photographs were taken of the cavitation cloud formations near the impeller vanes during operation in water at various pump inlet pressures and flow conditions. From these photographs (figs. 26 to 30 in ref. 1) it can be seen that, in general, ex-

tensive cavitation cloud formations occurred in the low-pressure regions near the inlet. Higher pressure regions showed considerably less cavitation.

After the impeller was run in potassium at 1400° F (1033° K) for 350 hours, impeller vanes were examined for cavitation damage. Severe vane damage occurred in the region of higher fluid pressure while little or no damage was noted near the inlet where lower fluid pressures were encountered. These results indicate that cavitation bubbles collapsing on a metal surface in a high-pressure region cause much more damage than bubbles that collapse on the metal surface in a lower pressure region. Thus, observations made in an actual pump application agree qualitatively with the results of our accelerated tests.

SUMMARY OF RESULTS

The effect of pressure on the resistance to cavitation damage of candidate materials for components of liquid-metal space power conversion systems was investigated. A vibratory apparatus was used. Three materials, L-605, Stellite 6B, and AISI 316 stainless steel were subjected to accelerated cavitation damage in 800° F (700° K) sodium under cover gas pressures of 1 to 4 atmospheres (1×10^5 to 4×10^5 N/m^2). The following results were obtained:

1. Increasing cover-gas pressure significantly increased cavitation damage to all materials. For example, an L-605 specimen tested under 1 atmosphere pressure (1×10^5 N/m^2) for 360 minutes exhibited

a volume loss of 10 cubic millimeters, as compared to 200 cubic millimeters after 360 minutes under 4 atmospheres (4×10^5 N/m^2). This result implies that in fluid systems where cavitation occurs in high-pressure regions, damage to components may be much greater than would normally be expected from cavitation tests conducted at atmospheric pressures.

2. Within the range of conditions (specimen size and cover-gas pressures) considered in this investigation, the steady-state volume-loss rate (based on total specimen area) for each material increased linearly with cover-gas pressure. When the volume-loss rate data were normalized to include only the heavily damaged area of the specimens, the steady-state volume-loss rate increased as a power function of pressure with the exponent going from 2.0 to 2.7.

3. The relative ranking of the materials with respect to resistance to cavitation damage was the same regardless of cover-gas pressure. (It was, in order of increasing damage, Stellite 6B, L-605 and AISI 316 stainless steel.) This result together with the fact that the damage rate increases with increasing pressure suggests that a greater number of materials may be evaluated in a given time at higher pressures than at atmospheric pressure.

4. Metallographic examination of axially sectioned specimens of all the materials tested revealed severe undercutting of the surface and transgranular cracking. Subsurface deformation was indicated in all materials by the appearance of slip bands. Stellite 6B showed extensive cracking of carbides beneath the surface, and L-605 exhibited some bending of twins near the surface.

REFERENCES

1. Kulp, R. S.; and Altieri, J. V.: Cavitation Damage of Mechanical Pump Impellers Operating in Liquid Metal Space Power Loops. Pratt and Whitney Aircraft (NASA CR-165), July 1965.

2. Smith, P. G.; DeVan, J. H.; and Grindell, A. G.: Cavitation Damage to Centrifugal Pump Impellers During Operation with Liquid Metals and Molten Salt at 1050-1400 F. J. Basic Eng., vol. 85, no. 3, Sept. 1963, pp. 329-337.

3. Hammitt, F. G.: Observations on Cavitation Damage in a Flowing System. J. Basic Eng., vol. 85, no. 3, Sept. 1963, pp. 347-359.

4. Young, Stanley G.; and Johnston, James R.: Accelerated Cavitation Damage of Steels and Superalloys in Liquid Metals. NASA TN D-3426, 1966.

5. Garcia, R.; Hammitt, F. G.; and Nystrom, R. E.: Comprehesive Cavitation Damage Data for Water, Mercury, and Lead-Bismuth Alloy Including Correlations with Material and Fluid Properties. Erosion by Cavitation or Impingement. Spec. Tech. Publ. 408, ASTM, 1967.

6. Thiruvengadam, A.; and Preiser, H. S.: Cavitation Damage in Liquid Metals. Rep. No. TR 467 (NASA CR-72035), Hydronautics, Inc., Nov. 29, 1965.

7. Knapp, Robert T.: Recent Investigations of the Mechanics of Cavitation Damage. Trans. ASME, vol. 77, no. 7, Oct. 1955, pp. 1045-1054.

8. Plesset, M. S.; and Ellis, A. T.: On the Mechanism of Cavitation Damage. Trans. ASME, vol. 77, no. 7, Oct. 1955, pp. 1055-1064.

9. Naude, Charl F.; and Ellis, Albert T.: On the Mechanism of Cavitation Damage by Non-Hemispherical Cavities Collapsing in Contact with a Solid Boundary. J. Basic Eng., vol. 83, no. 4, Dec. 1961, pp. 648-656.

10. Knapp, R. T.; and Hollander, A.: Laboratory Investigations of the Mechanism of Cavitation. Trans. ASME, vol. 70, no. 5, July 1948, pp. 419-435.

11. Peters, H.; and Rightmire, B. G.: Cavitation Study by the Vibratory Method. Proceedings of the Fifth International Congress for Applied Mechanics. J. P. Den Hartog and H. Peters, eds., John Wiley and Sons, Inc., 1939, pp. 614-616.

12. Weatherford, W. D., Jr.; Tyler, John C.; and Ku, P. M.: Properties of Inorganic Working Fluids and Coolants for Space Applications. (WADC TR 59-598), Southwest Research Inst., Dec. 1959.

13. Anon.: Wear Resistant Alloys. Bull. No. F 30-1-33-A, Haynes Stellite Co., 1962.

14. Weiss, V.; and Sessler, J. G., eds.: Aerospace Structural Metals Handbook. Third rev., Syracuse University Press, 1966.

TABLE I. - NOMINAL CHEMICAL COMPOSITIONS OF TEST MATERIALS

Material	Composition, weight percent											
	Iron	Nickel	Cobalt	Chromium	Molybdenum	Tungsten	Carbon	Manganese	Silicon	Phosphorous	Sulfur	Copper
Stellite 6B[a]	[b]3	[b]3	Bal.	30	[b]1.5	4.5	1.1	[b]2	[b]2	-----	-----	-----
L-605 AMS 5759B[c]	[b]3	10	Bal.	20	----	15	.1	1.5	[b]1.0	[b]0.04	[b]0.03	-----
AISI 316 stainless steel AMS 5648C[c]	Bal.	13	---	18	2.5	----	.08	1.6	[b]1.0	[b].04	[b].03	[b]0.50

[a]Ref. 13.
[b]Maximum.
[c]Aerospace Materials Specifications.

TABLE II. - HEAT TREATMENT, DENSITIES, AND 800° F (700° K)

MECHANICAL PROPERTIES OF TEST MATERIALS

Material	Heat treatment	Density		Ultimate tensile strength		Yield strength		Elongation, percent
		$lb/in.^3$	kg/m^3	psi	N/m^2	psi	N/m^2	
Stellite 6B[a]	Solution heat treated at 2250° F (1506° K); air cooled	0.303	8.38×10^3	138 000	9.5×10^8	71 000	4.9×10^8	29.0
L-605[b]	Solution heat treated at 2250° F (1560° K); water quenched	0.330	9.13×10^3	119 000	8.2×10^8	35 000	2.4×10^8	75.0
AISI 316[b] stainless steel	Annealed	0.288	7.98×10^3	70 000	4.8×10^8	28 000	1.9×10^8	40.0

[a]Ref. 13.
[b]Ref. 14.

TABLE III. - TEST CONDITIONS

[Temperature, 800±10° F (700° K); fluid, sodium (99.95 percent purity); frequency, 25 000 ±500 Hz; amplitude, 0.00175±0.00005 in. (4.45×10^{-2} mm).]

Material	Pressure[a]		Total test time, min
	atm	N/m^2	
Stellite 6B	1.0	1.0×10^5	600
	2.7	2.7	540
	4.0	4.0	480
L-605	1.0	1.0×10^5	360
	2.0	2.0	
	3.0	3.0	
	4.0	4.0	
AISI 316 stainless steel	1.0	1.0×10^5	240
	2.7	2.7	300
	4.0	4.0	240

[a]Nominal pressure, ±0.02 atmosphere.

TABLE IV. - SUMMARY OF CAVITATION TEST DATA

Material	Cover-gas pressure		Time, min										Steady-state volume-loss rate, mm^3/hr
			60	120	180	240	300	360	420	480	540	600	
	atm	N/m^2	Volume loss, mm^3										
Stellite 6B	1.0	1.0×10^5	----	(0.04)	(0.13)	0.4	1.1	1.6	2.1	2.6	----	3.6	0.5
	2.7	2.7	----	16.8	27.0	39.0	49.2	54.8	60.1	65.5	69.8	---	5.0
	4.0	4.0	17.1	29.0	36.1	43.3	51.7	62.1	----	80.6	----	---	7.2
L-605	1.0	1.0×10^5	0.1	1.0	3.0	5.0	7.5	10.0	----	----	----	---	2.4
	2.0	2.0	8.7	25.3	38.8	48.3	59.3	70.9	----	----	----	---	10.5
	[a]3.0	[a]3.0	27.1	49.9	-----	-----	-----	-----	----	----	----	---	----
	[b]3.0	[b]3.0	----	61.3	79.1	95.5	113	141	----	----	----	---	17.7
	4.0	4.0	46.6	74.5	102	130	160	201	----	----	----	---	27.5
316 stainless steel	1.0	1.0×10^5	3.6	8.6	13.8	18.0	-----	-----	----	----	----	---	4.2
	2.7	2.7	----	63.3	90.8	119	153	-----	----	----	----	---	27.2
	4.0	4.0	71.0	124	165	209	-----	-----	----	----	----	---	41.0

[a]First specimen.
[b]Second specimen.

TABLE V. -DETERMINATION OF NORMALIZIED STEADY

STATE VOLUME LOSS RATE

Material	Pressure		Heavy damage area,[a] mm^2	Normalizing factor[b]	Normalized steady-state volume-loss rate,[c] mm^3/hr
	atm	N/m^2			
Stellite 6B	1.0	1.0×10^5	140	1.2	0.6
	2.7	2.7	96	1.7	8.5
	4.0	4.0	45	3.6	26
L-605	1.0	1.0×10^5	150	1.1	2.6
	2.0	2.0	140	1.2	13
	3.0	3.0	99	1.6	28
	4.0	4.0	80	2.0	55
AISI 316 stainless steel	1.0	1.0×10^5	130	1.2	5.2
	2.7	2.7	96	1.7	46
	4.0	4.0	74	2.2	90

[a](Average diameter of damaged area)$^2 \times \pi/4$.
[b]Ratio of total specimen area to heavily damaged area.
[c]Steady-state volume-loss rate (from table IV) × normalizing factor.

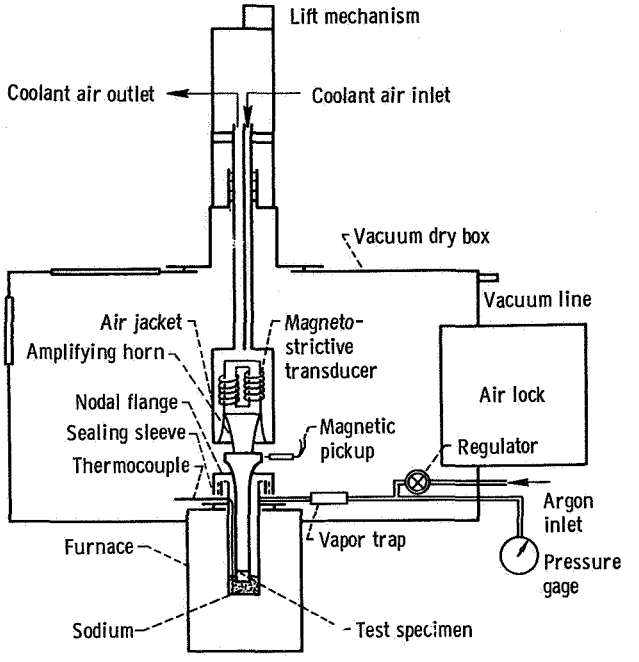

Figure 1. - Schematic diagram of cavitation apparatus.

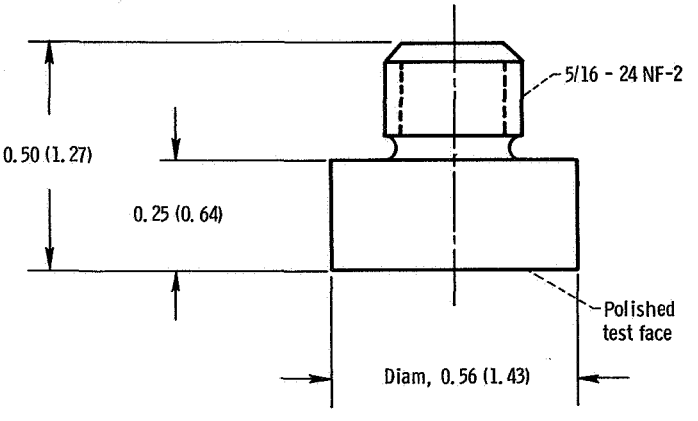

Figure 2. - Cavitation test specimen. (Dimensions in inches (cm).)

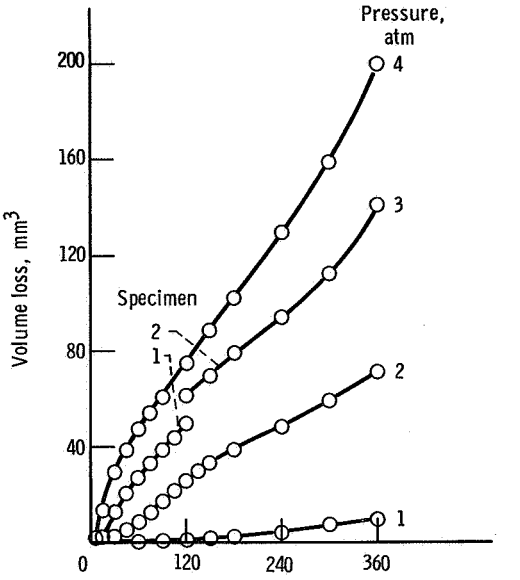

(a) Cumulative cavitation damage.

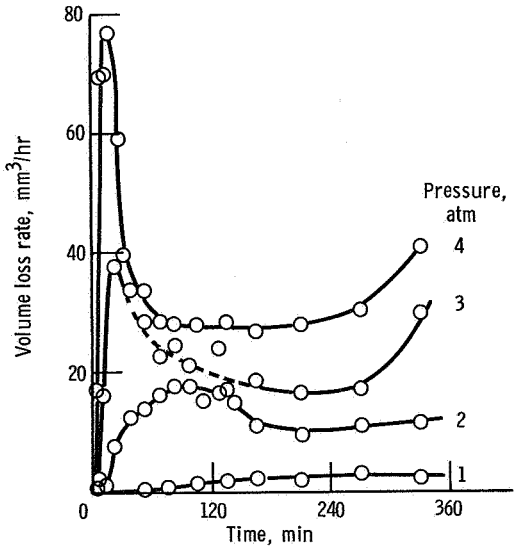

(b) Rate of cavitation damage.

Figure 3. - Cavitation damage of L-605 tested in 800° F (700° K) sodium at various pressures (1 atm = ~10^5 N/m^2).

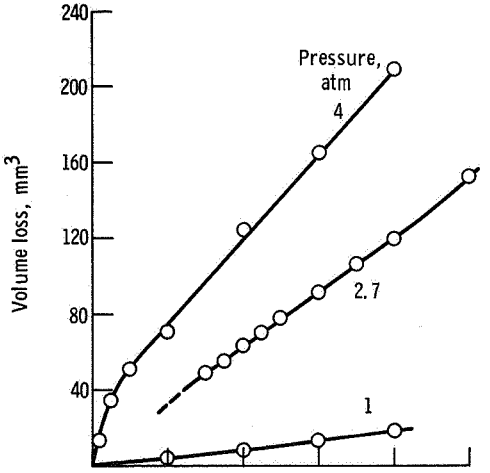

(a) Cumulative cavitation damage.

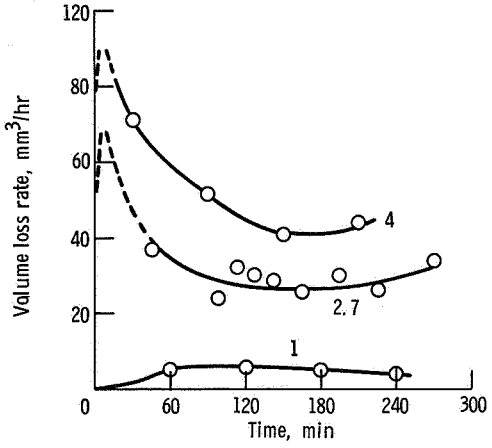

(b) Rate of cavitation damage.

Figure 4. - Cavitation damage of AISI type 316 stainless-steel tested in 800° F (700° K) sodium at various temperatures (1 atm =~10^5 N/m^2).

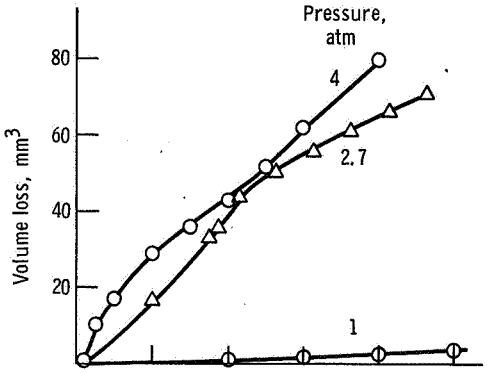

(a) Cumulative cavitation damage.

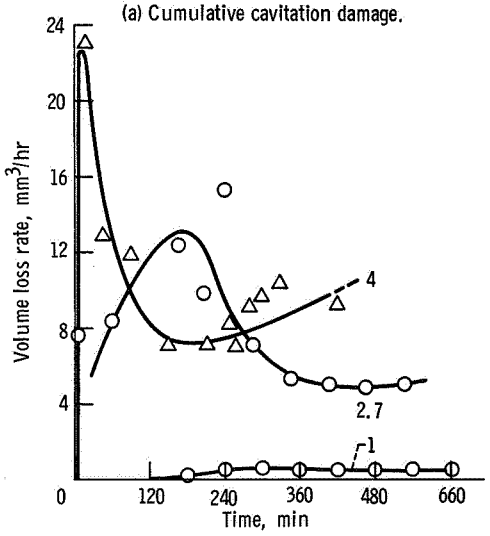

(b) Rate of cavitation damage.

Figure 5. - Cavitation damage of Stellite 6B in 800° F (700° K) sodium at various pressures (1 atm =~10^5 N/m^2).

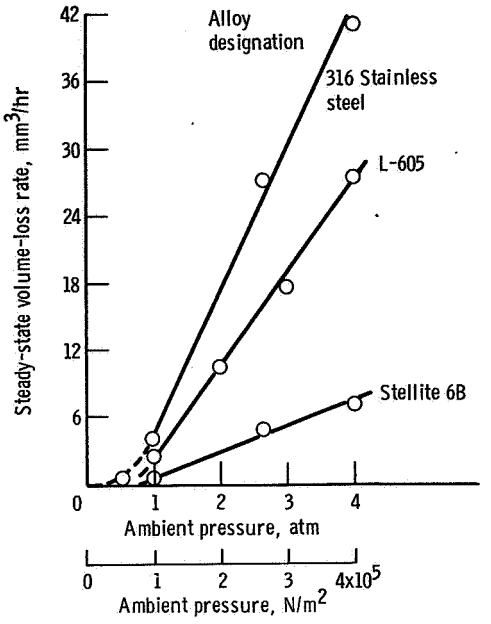

Figure 6. - Relation between cavitation damage rate and ambient pressure for materials tested in 800° F (700° K) sodium.

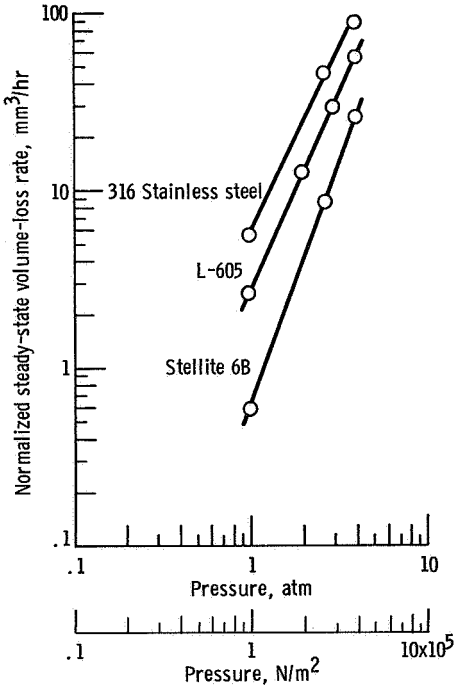

Figure 7. - Relation of cavitation damage, normalized to area basis, to ambient pressure for materials tested in 800° F (700° K) sodium.

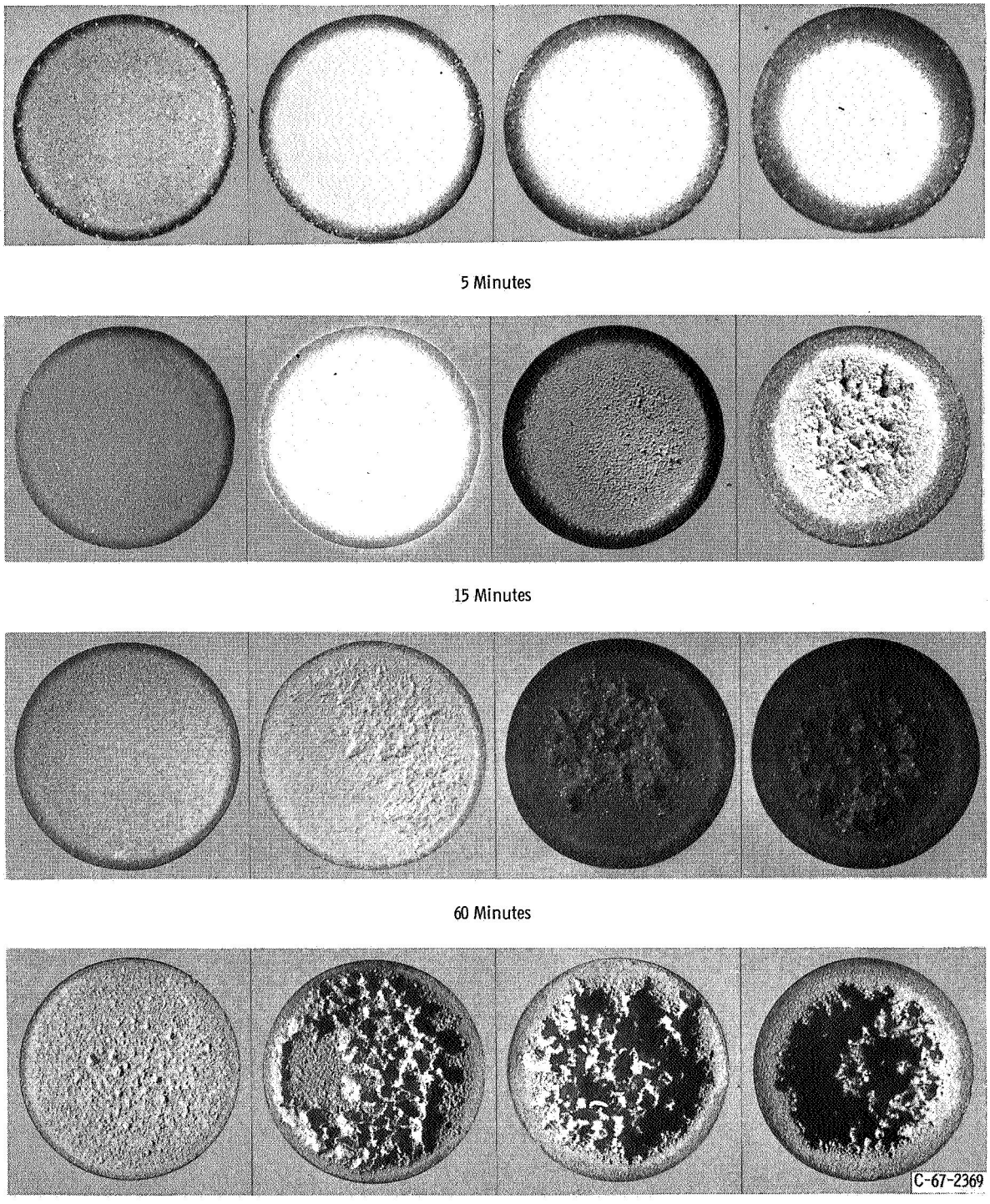

Figure 8. - Damaged surfaces of L-605 specimens after exposure to cavitation in sodium at 800° F (700° K) at various times and pressures (1 atm = ~10^5 N/m^2).

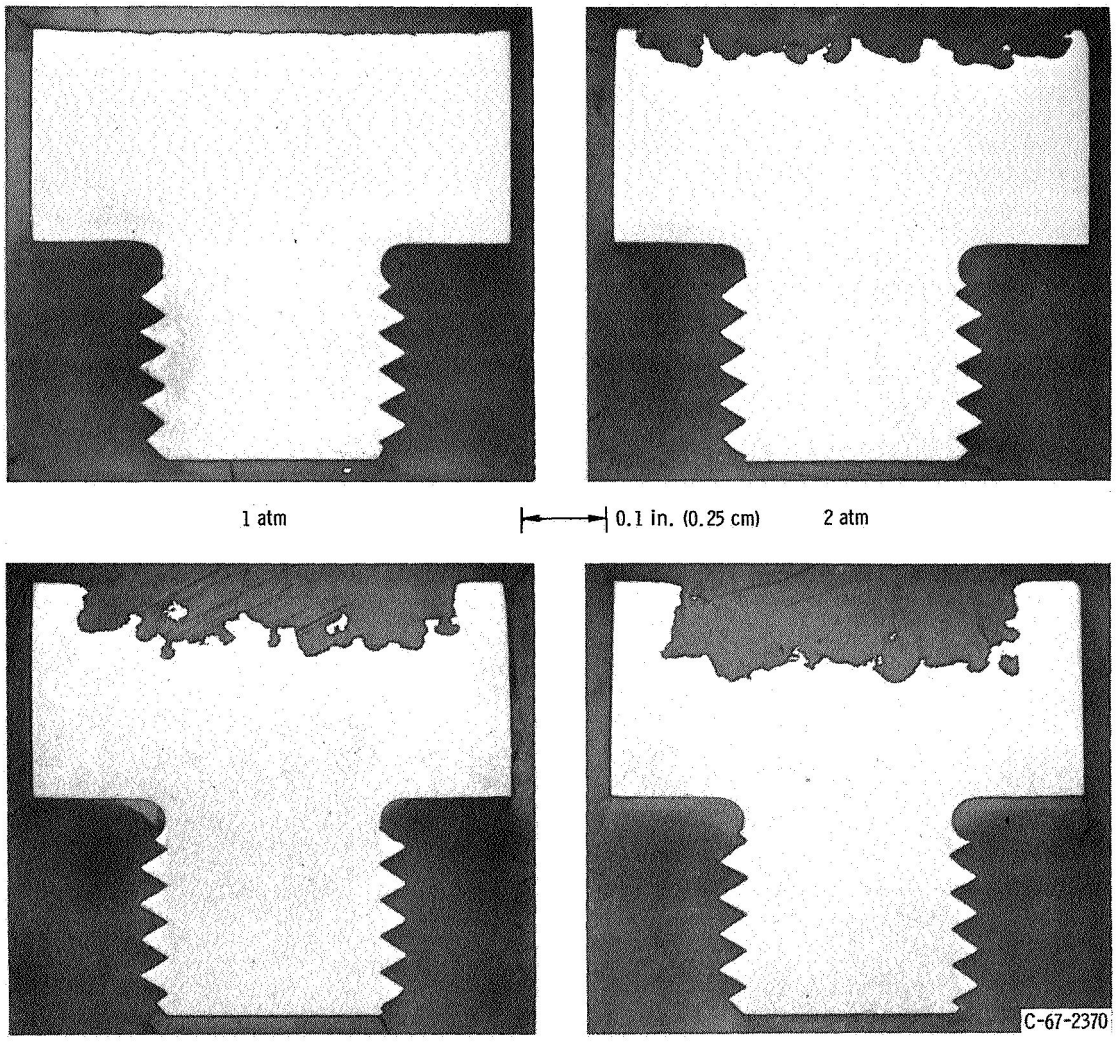

Figure 9. - Sections of L-605 specimens after exposure to cavitation in sodium at 800° F (700° K) for 360 minutes at various pressures. (Unetched) (1 atm = ~10^5 N/m^2).

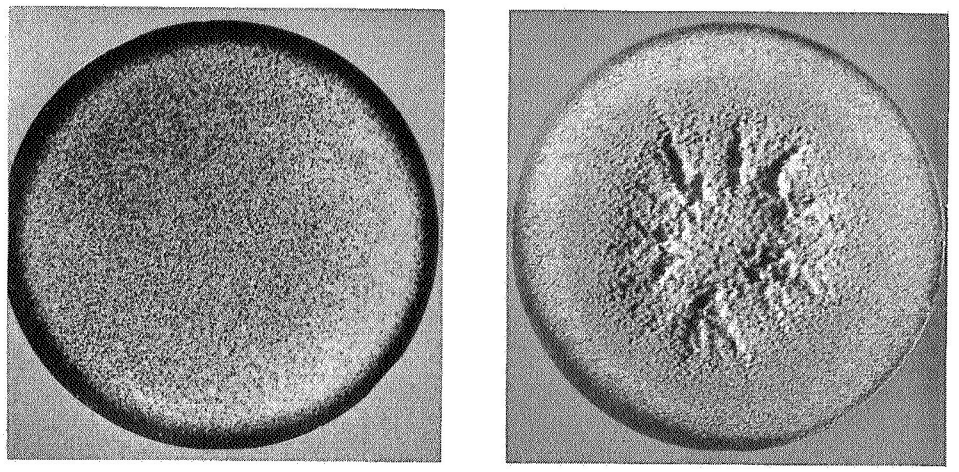

0.1 in. (0.25 cm)

5 Minutes

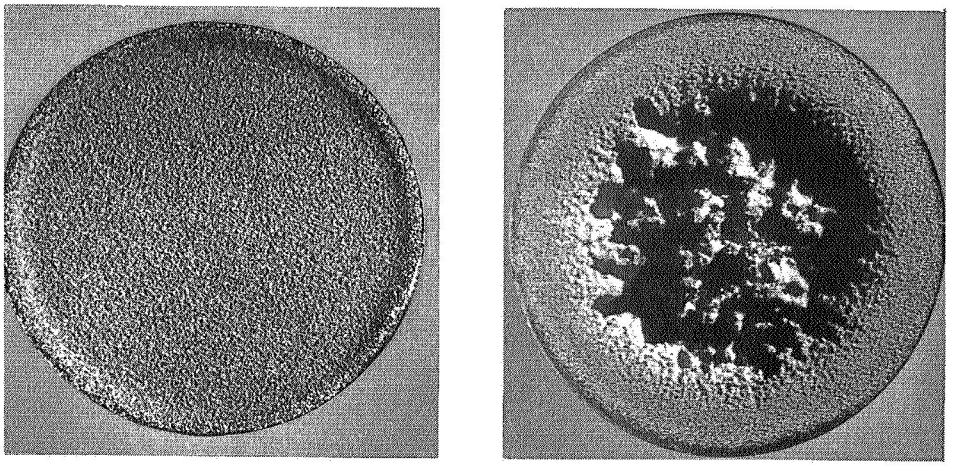

60 Minutes

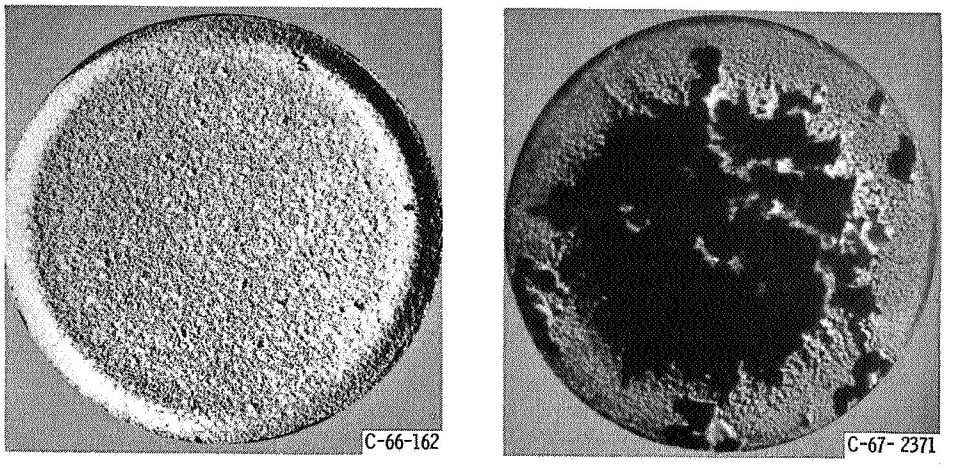

240 Minutes

1 4

Pressure, atm

Figure 10. - Damaged surfaces of AISI 316 stainless-steel specimens after exposure to cavitation in sodium at 800° F (700° K) at various times and pressures (1 atm = ~10^5 N/m^2).

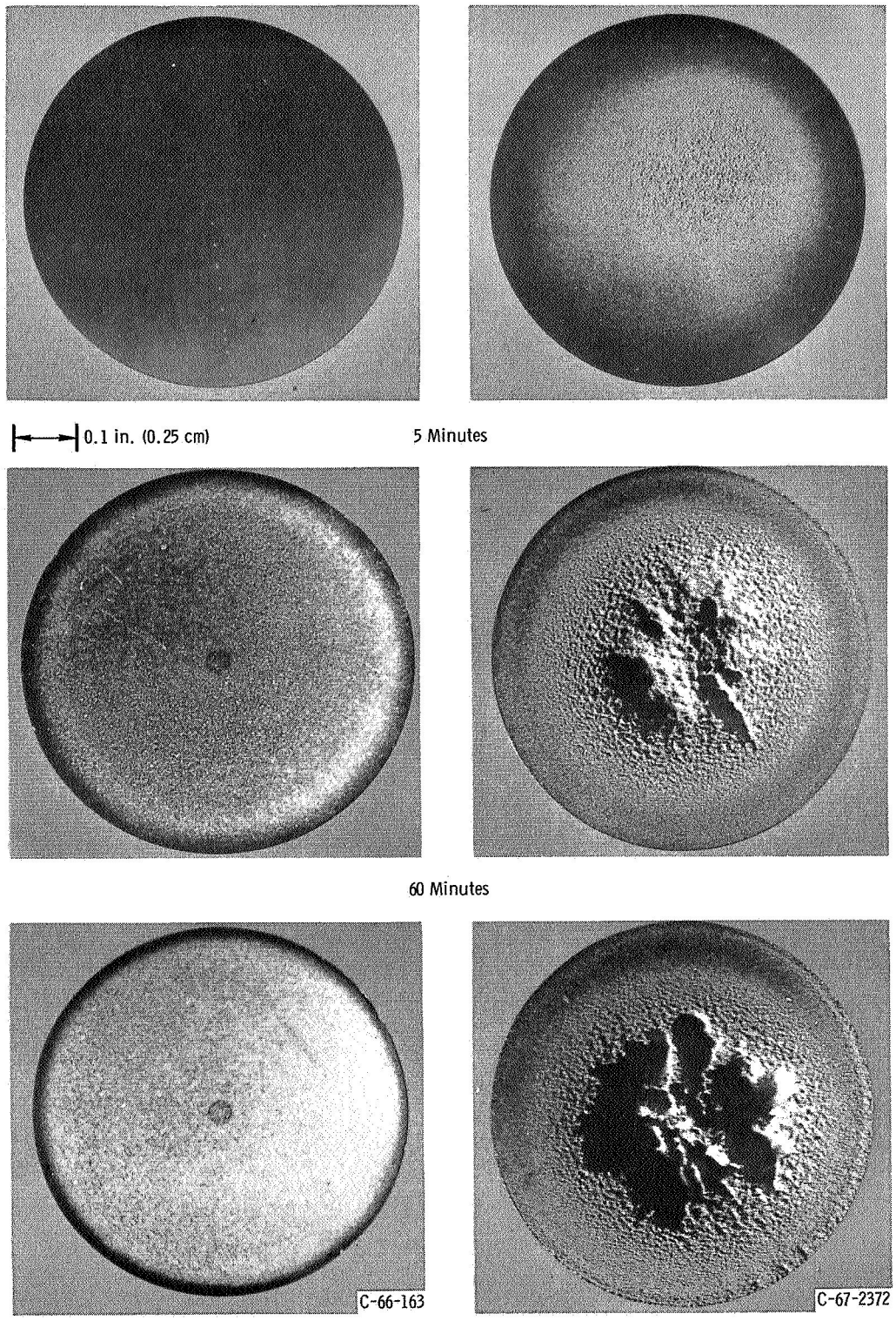

Figure 11. - Damaged surfaces of Stellite 6B specimens after exposure to cavitation in sodium at 800° F (700° K) at various times and pressures (1 atm = $\sim 10^5$ N/m^2).

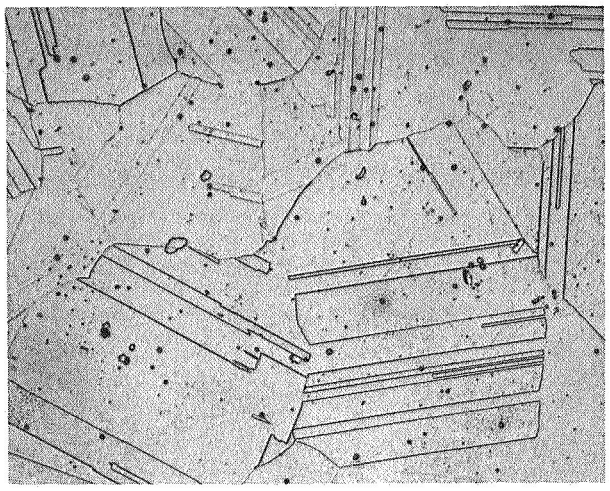

0.001 in. (0.0025 cm)

Untested - etched.

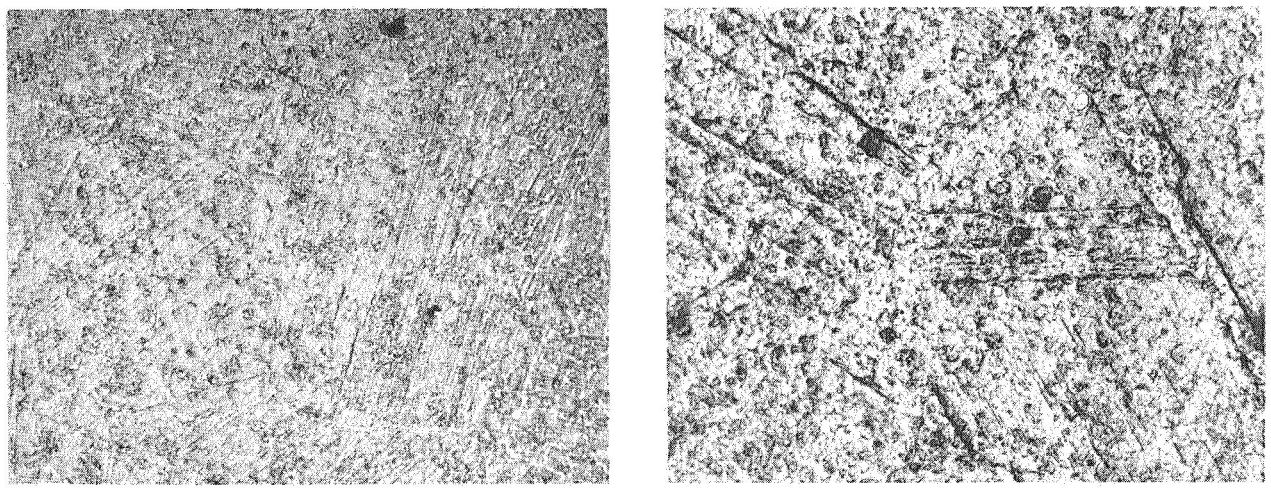

5 Minutes

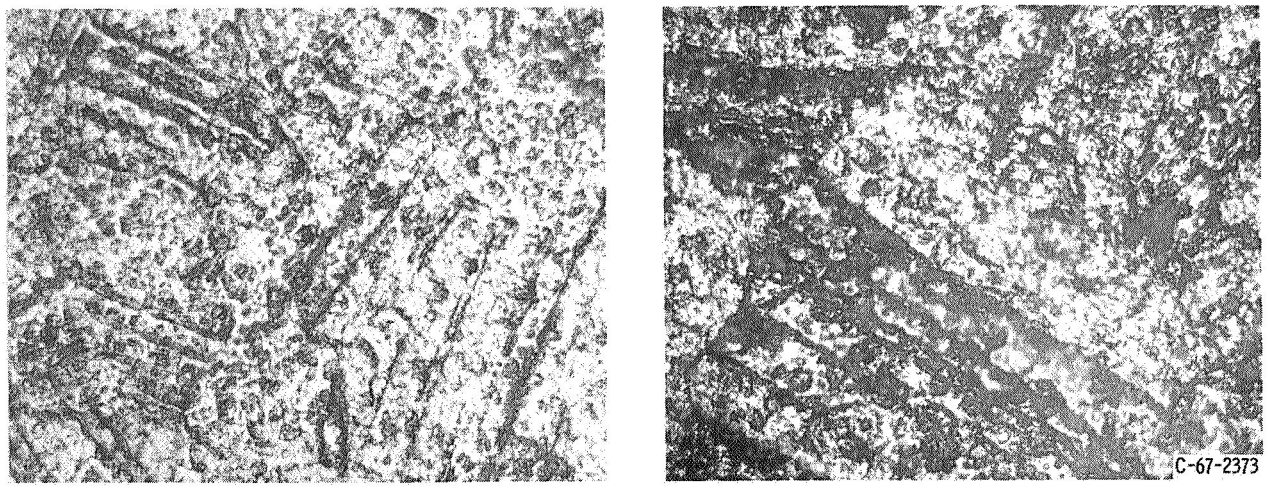

15 Minutes

1 2

Pressure, atm

Figure 12. - Photomicrographs of damaged surfaces of L-605 specimens exposed to cavitation in sodium at 800° F (700° K) (1 atm = ~10^5 N/m^2), X250.

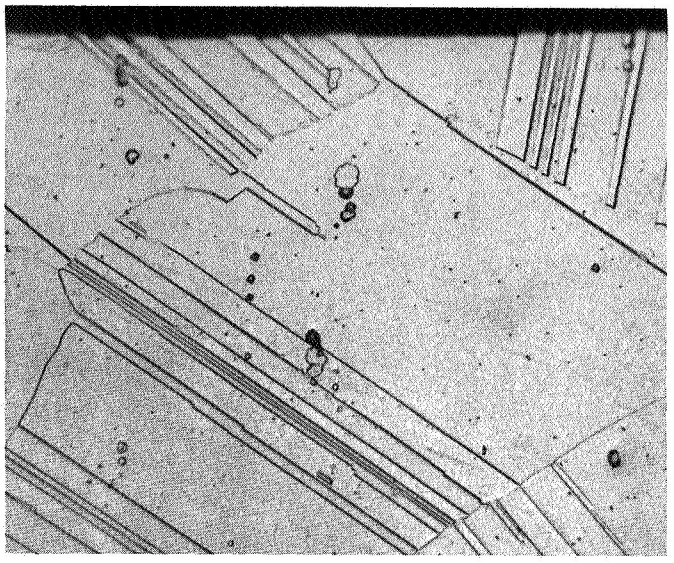

As-received, X500.

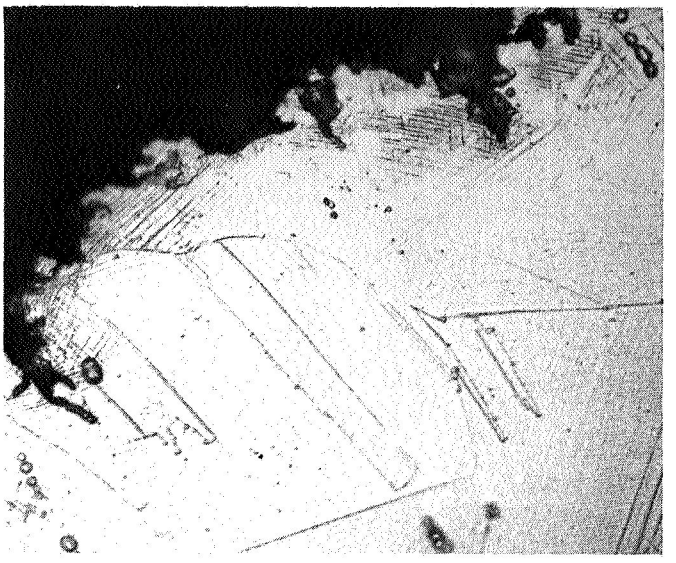

0.001 in. (0.0025 cm)

360-Minute exposure at 1 atmosphere, X500.

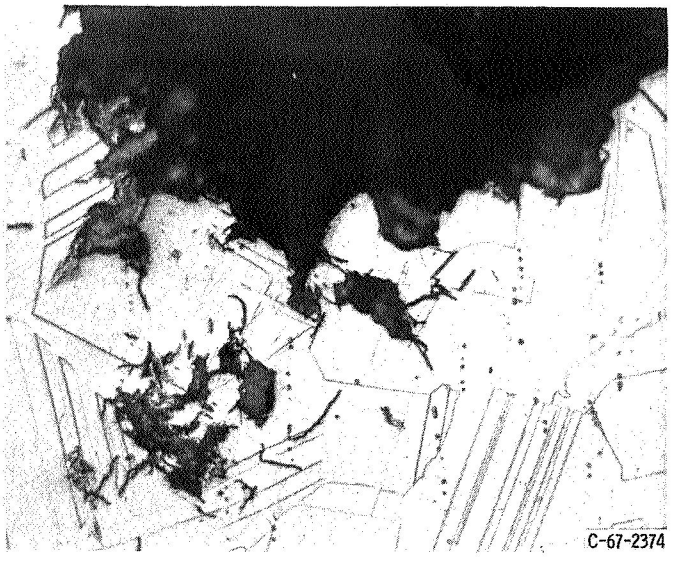

360-Minute exposure at 4 atmospheres, X250.
(a) L-605.

0.001 in. (0.0025 cm)

Figure 13. - Photomicrographs of sectioned specimens before and after exposure to cavitation in sodium at 800° F (700° K) (1 atm = ~10^5 N/m^2).

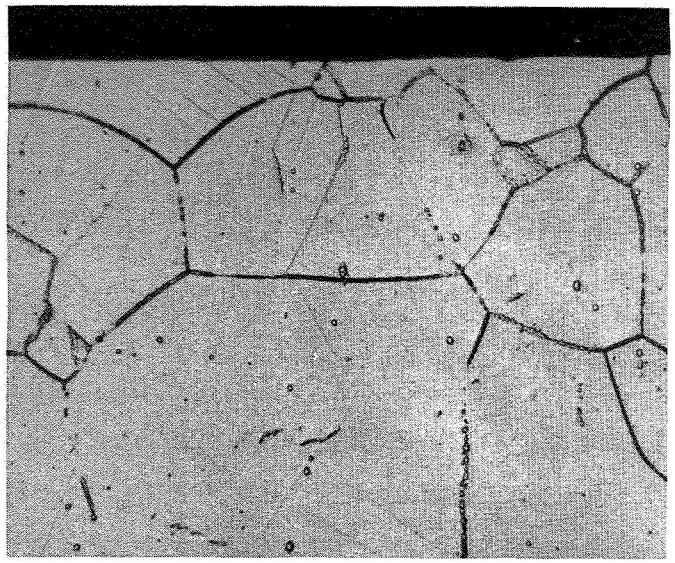

As-received, X500.

240-Minute exposure at 1 atmosphere, X500.

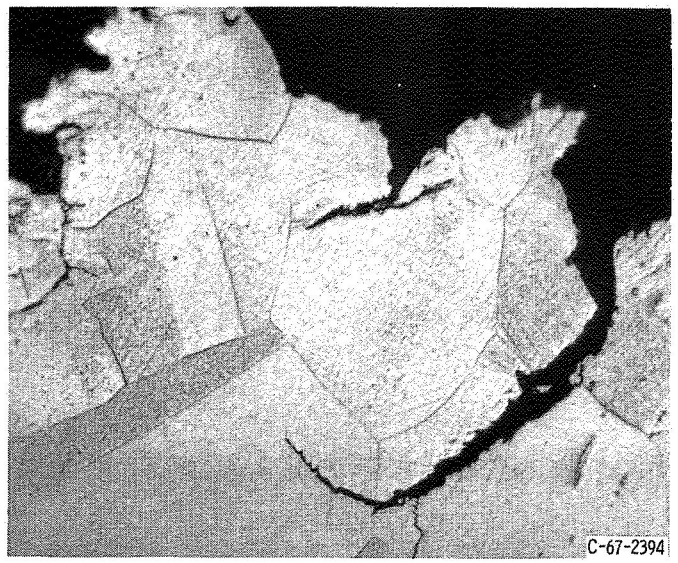

240-Minute exposure at 4 atmospheres, X500.
(b) AISI 316 stainless steel.

0.001 in. (0.0025 cm)

Figure 13. - Continued.

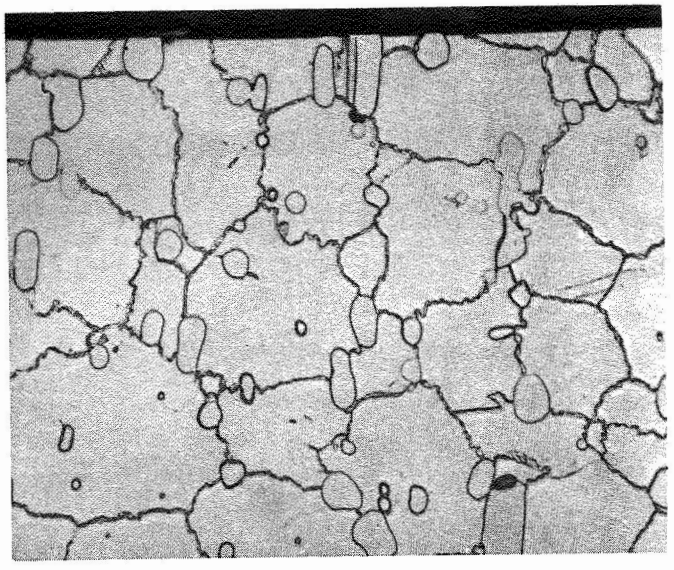

As-received, X500.

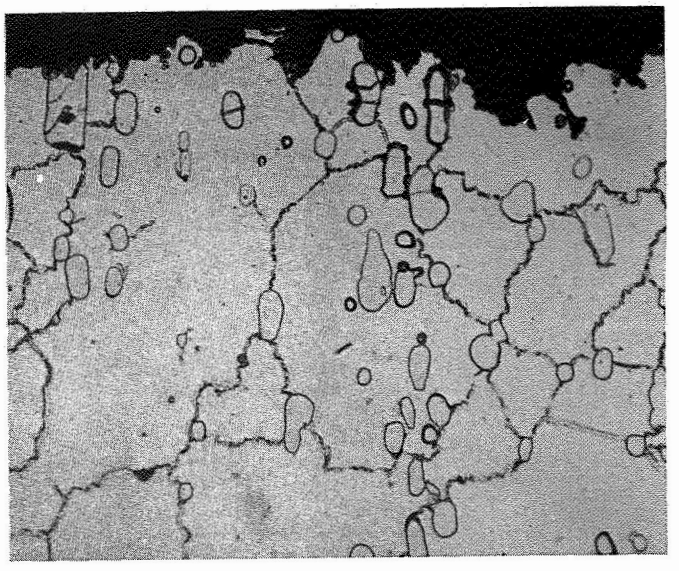

600-Minute exposure at 1 atmosphere, X500.

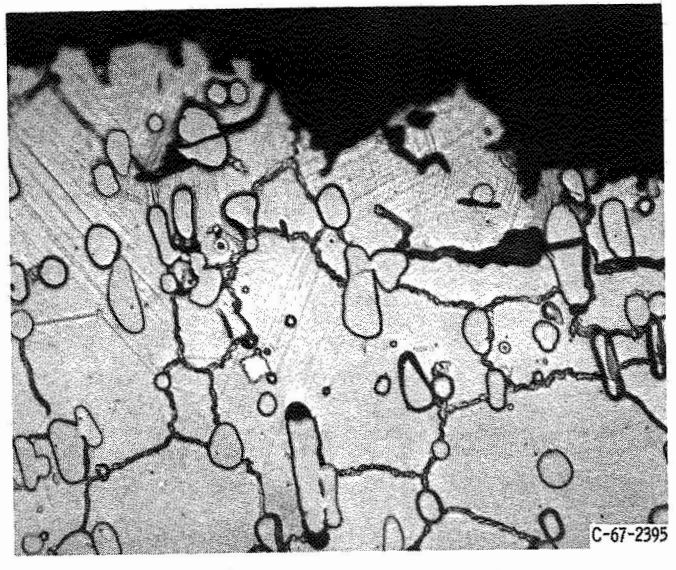

480-Minute exposure at 4 atmospheres, X500.
(c) Stellite 6B.

0.001 in. (0.0025 cm)

Figure 13. - Concluded.